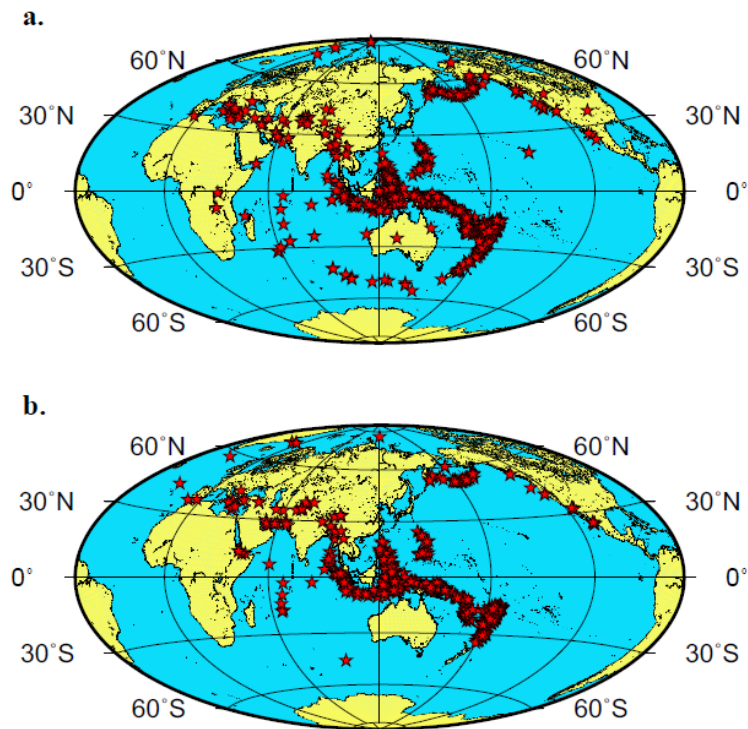1   **Supporting Information for "Shear wave velocity structure beneath Northeast**

2   **China from joint inversion of receiver functions and Rayleigh wave group**

3   **velocities: Implications for intraplate volcanism"**

4

5   Figure S1. (a) Global distribution of earthquakes (2016–2019, red stars) for our receiver

6   function analysis at the permanent CEA stations. (b) Global distribution of earthquakes

7   (between 2009.09 and 2011.08, red stars) for obtaining receiver functions at the

8   temporary NECESSArray sites.

9
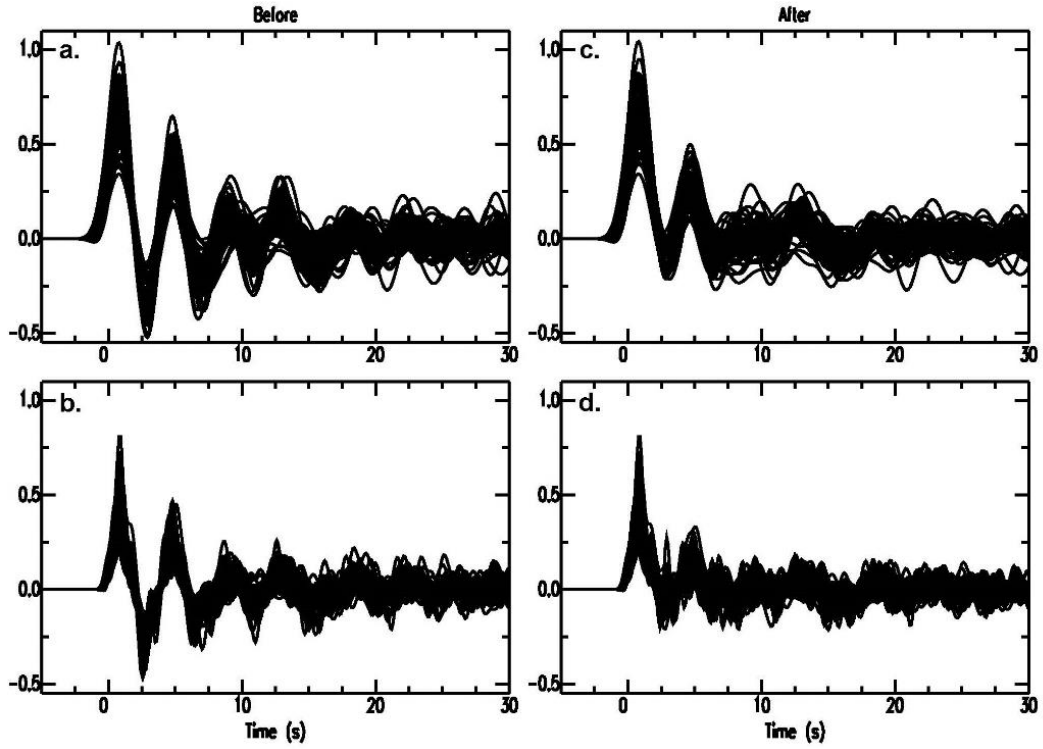
Figure S2. Radial receiver functions at low (fc ≤ 0.50 Hz, Gaussian width α = 1.0) and

high (fc ≤ 1.25 Hz, Gaussian width α = 2.5) frequency bands recorded by station NEA7

(located in the SLB and marked in Figure 2) are plotted in panel a and b, respectively.

Panel c and d exhibit the resulting receiver functions at the two frequency ranges after
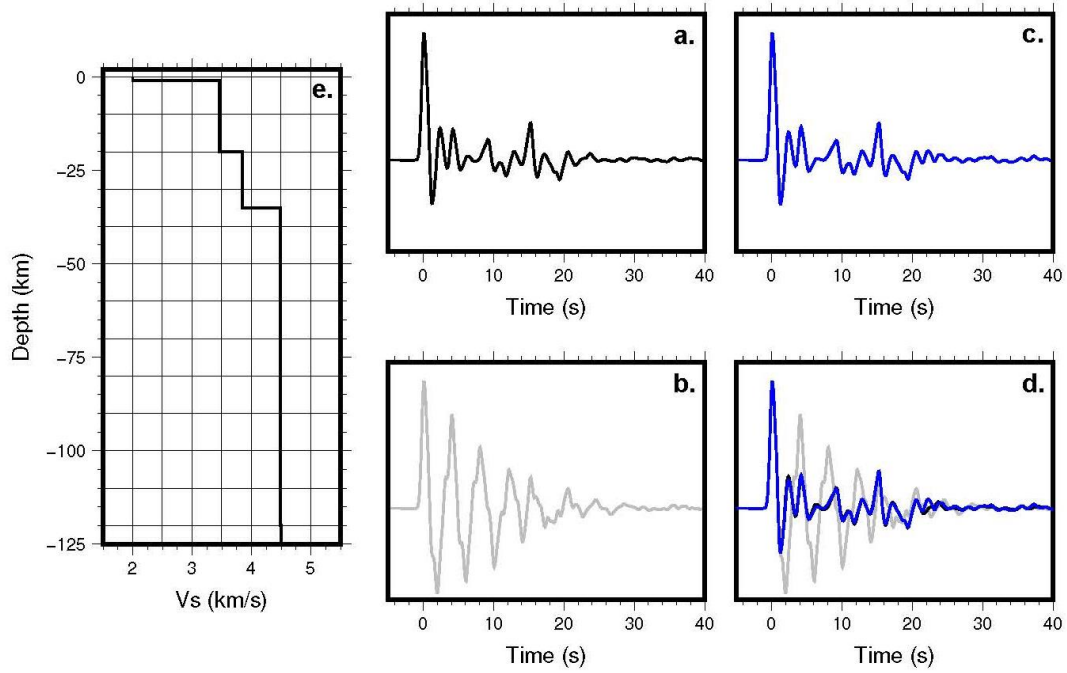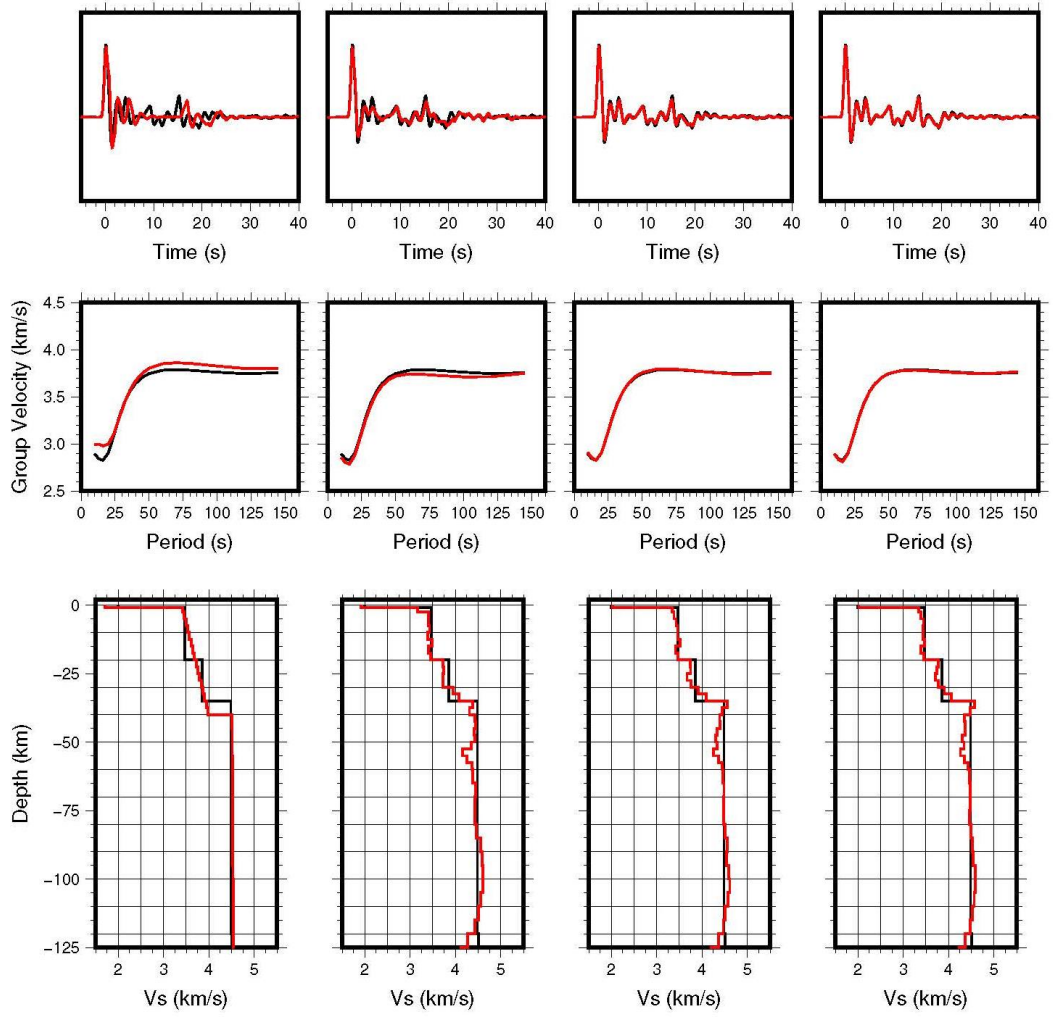
applying the resonance removal filter.

15

Figure S3. (a) Synthetic receiver function (ray-parameter 0.05 s/km, at Gaussian width

of α = 2.5) corresponding to the true model in panel (e). Note that a 1.0 km thick

sedimentary layer is presumed and the primary P-to-S phases triggered by the

sedimentary structure are likely between 1 and 3 s. However, it does not account for

the complex situation that energy reverberating within the sedimentary layer (i.e.,

multiples of converted shear waves). (b) Synthetic receiver function corresponding to

the same true model, but including strong near-surface reverberations of converted

shear phases. It is defined by the equation (2) in Yu et al. (2015). (c) Resulting receiver

function after applying the resonance removal filter on the time series in panel (b). (d)

Comparison between the synthetic receiver function without near-surface

reverberations (black), the synthetic receiver function with strong near-surface

multiples (gray), and the resulting receiver function after applying the resonance

removal filter (blue). The blue trace is quite consistent with the black one (in both

amplitude and lag time), which illustrates that the resonance removal filter effectively

removes the near-surface multiples of converted shear phases and successfully recovers

31   the right signals from deep interfaces.

32
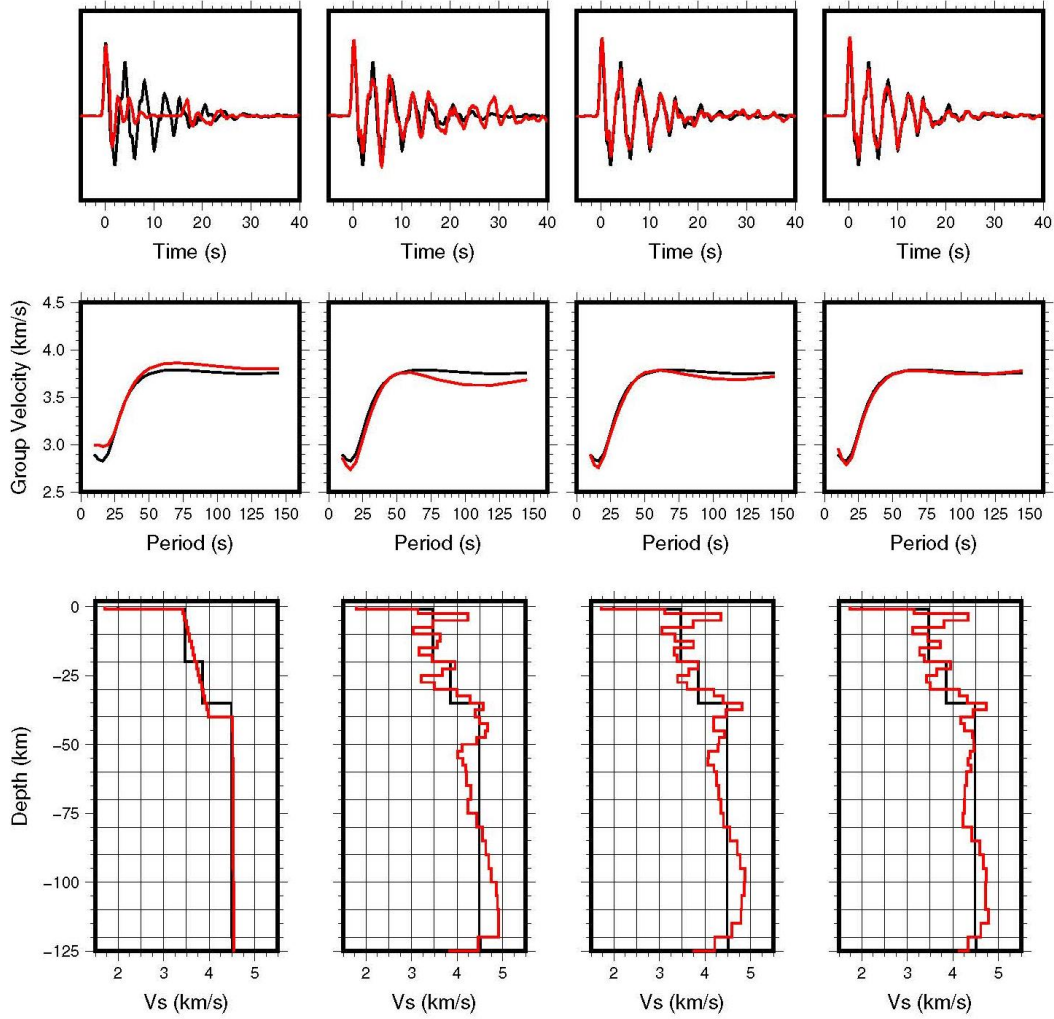
Figure S4. A synthetic test for joint inversion. Theoretical receiver function with strong

near-surface reverberations (the one in Figure S3b) and Rayleigh wave group velocity

dispersion curve that are corresponding to the true model (black) are represented by

black lines. Evolution of the iterated solutions and the corresponding predicted data are

shown by red lines. Note that the joint inversion converges to a solution, which however

contains many artifacts and unsuccessfully recovers the true model.

39

Figure S5. The resulting receiver function after the application of the resonance removal filter (the one in Figure S3c) is inverted jointly with synthetic Rayleigh wave dispersion data (black). Evolution of the iterated solutions and the predicted data are displayed by red lines. The inversion recovers the true model in three iterations.

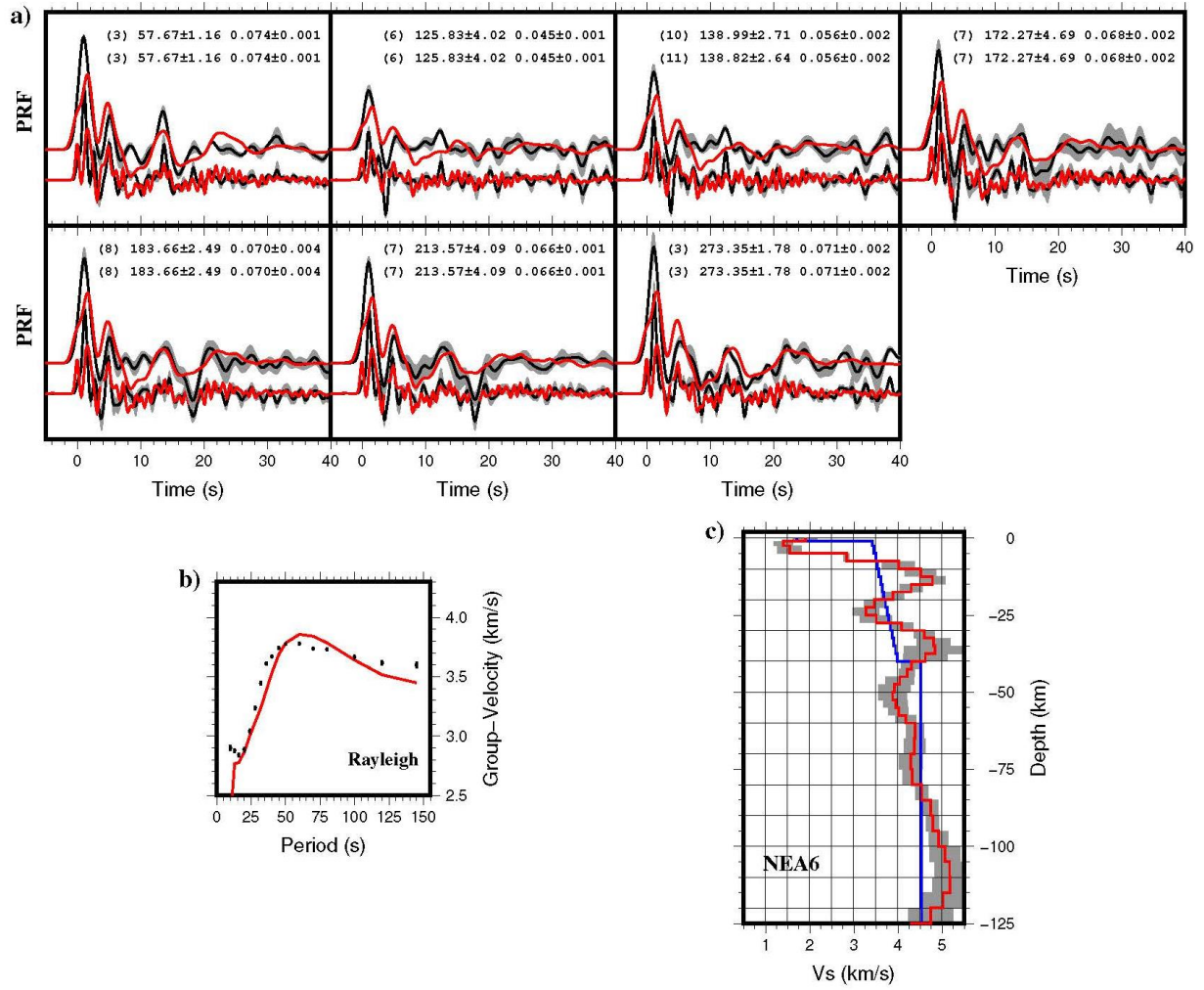a)

| (3) 57.67±1.16 0.074±0.001 | (6) 125.83±4.02 0.045±0.001 | (10) 138.99±2.71 0.056±0.002 | (7) 172.27±4.69 0.068±0.002 |
| (3) 57.67±1.16 0.074±0.001 | (6) 125.83±4.02 0.045±0.001 | (11) 138.82±2.64 0.056±0.002 | (7) 172.27±4.69 0.068±0.002 |

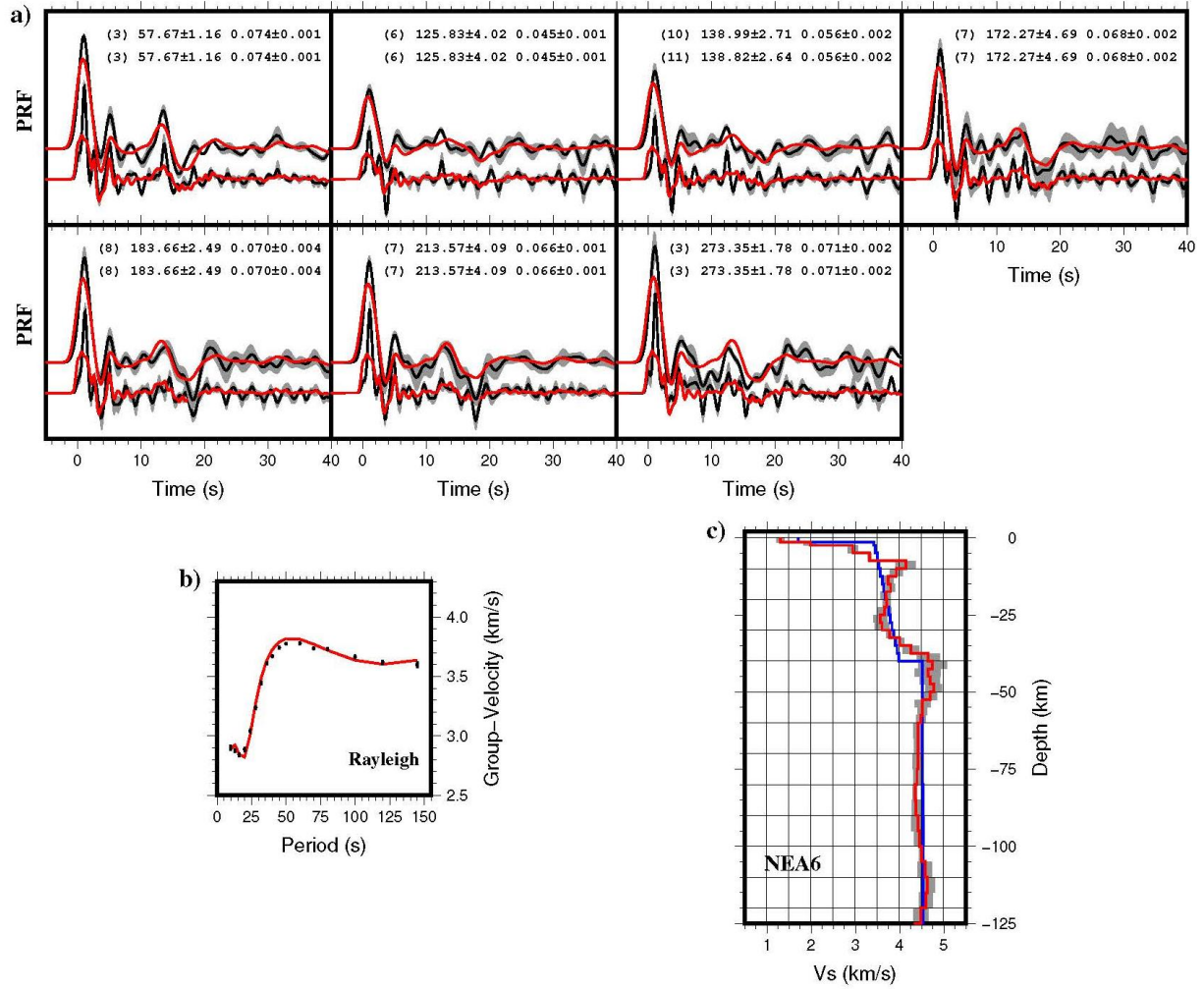| (8) 183.66±2.49 0.070±0.004 | (7) 213.57±4.09 0.066±0.001 | (3) 273.35±1.78 0.071±0.002 |
| (8) 183.66±2.49 0.070±0.004 | (7) 213.57±4.09 0.066±0.001 | (3) 273.35±1.78 0.071±0.002 |
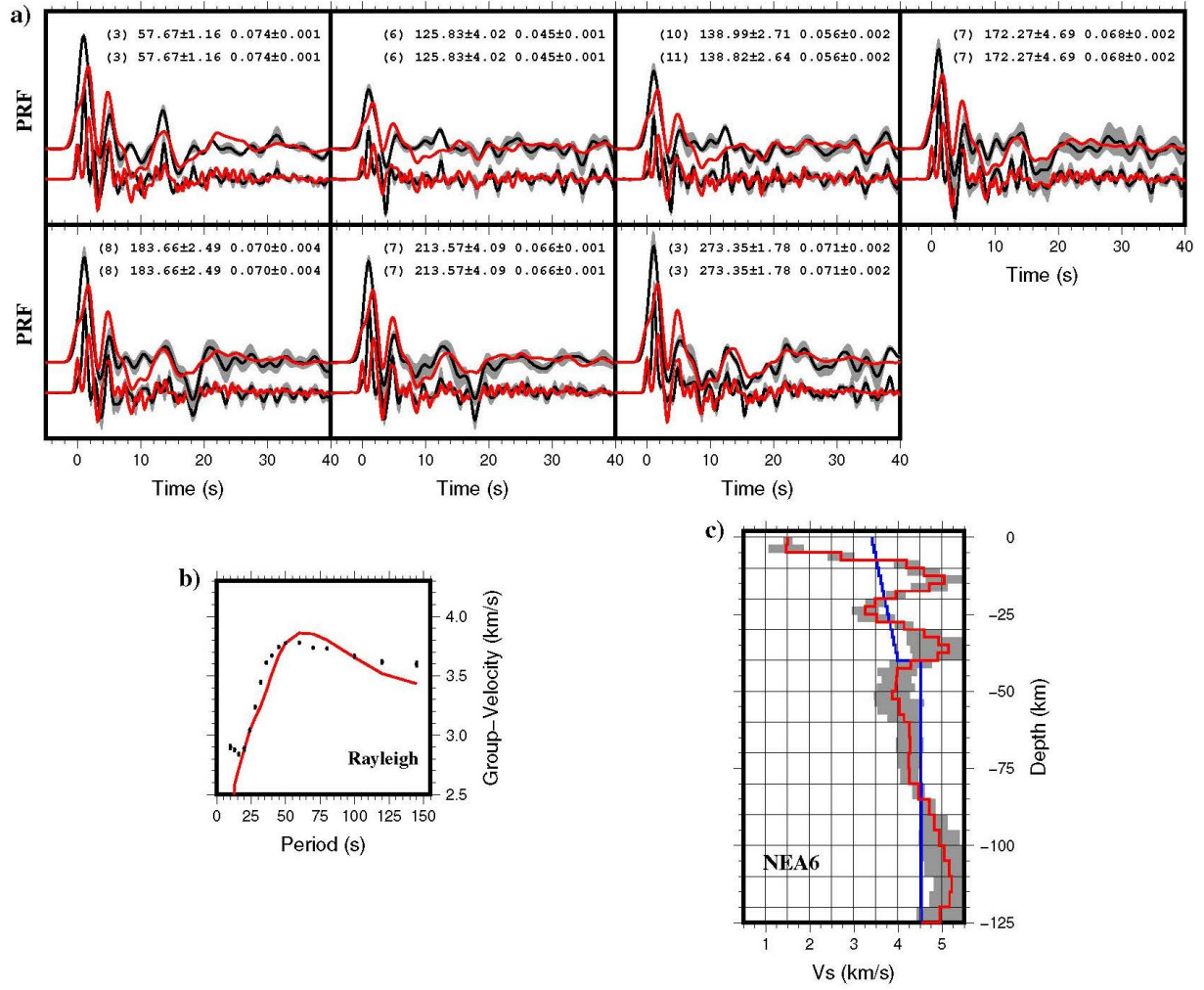
Figure S6. Unsuccessful joint inversion at station NEA6. The initial model (blue in panel c) that does not include a sedimentary layer is employed. Note that the solution (red in panel c) driven away from the convergence and the poor data fitting in both receiver functions (panels a) and Rayleigh wave dispersion velocities (panel b).

a)

(3) 57.67±1.16 0.074±0.001
(3) 57.67±1.16 0.074±0.001

(6) 125.83±4.02 0.045±0.001
(6) 125.83±4.02 0.045±0.001

(10) 138.99±2.71 0.056±0.002
(11) 138.82±2.64 0.056±0.002

(7) 172.27±4.69 0.068±0.002
(7) 172.27±4.69 0.068±0.002

(8) 183.66±2.49 0.070±0.004
(8) 183.66±2.49 0.070±0.004

(7) 213.57±4.09 0.066±0.001
(7) 213.57±4.09 0.066±0.001

(3) 273.35±1.78 0.071±0.002
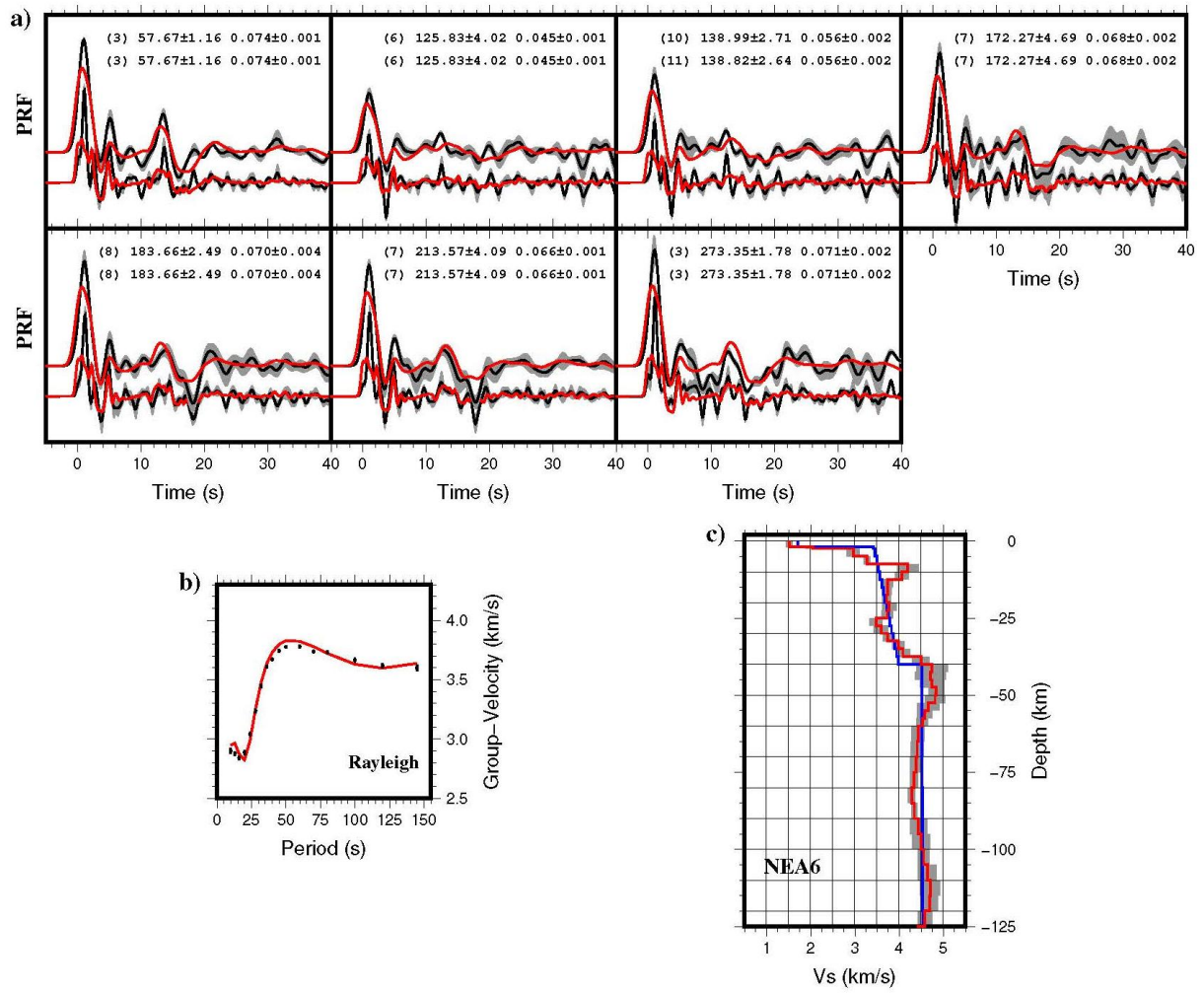(3) 273.35±1.78 0.071±0.002

PRF

Time (s)

b)

Rayleigh

c)

NEA6

Figure S7. Joint inversion at NEA6, but applying a starting model with a 1.0 km thick sedimentary layer (blue in panel c). The inversion is still unsuccessful.

7

a)

| (3) 57.67±1.16 0.074±0.001 | (6) 125.83±4.02 0.045±0.001 | (10) 138.99±2.71 0.056±0.002 | (7) 172.27±4.69 0.068±0.002 |
| (3) 57.67±1.16 0.074±0.001 | (6) 125.83±4.02 0.045±0.001 | (11) 138.82±2.64 0.056±0.002 | (7) 172.27±4.69 0.068±0.002 |

| (8) 183.66±2.49 0.070±0.004 | (7) 213.57±4.09 0.066±0.001 | (3) 273.35±1.78 0.071±0.002 |
| (8) 183.66±2.49 0.070±0.004 | (7) 213.57±4.09 0.066±0.001 | (3) 273.35±1.78 0.071±0.002 |

b) Rayleigh

c) NEA6

53 Figure S8. Joint inversion at NEA6, but employing an initial model with a 1.5 km thick
54 sedimentary layer (blue in panel c). This case is successful. The inverted S velocity
55 model is displayed in panel c. Note that the excellent match between predicted and
56 observed data in both receiver functions (panels a) and dispersion curve (panel b).

a)

(3) 57.67±1.16 0.074±0.001
(3) 57.67±1.16 0.074±0.001

(6) 125.83±4.02 0.045±0.001
(6) 125.83±4.02 0.045±0.001

(10) 138.99±2.71 0.056±0.002
(11) 138.82±2.64 0.056±0.002

(7) 172.27±4.69 0.068±0.002
(7) 172.27±4.69 0.068±0.002

(8) 183.66±2.49 0.070±0.004
(8) 183.66±2.49 0.070±0.004

(7) 213.57±4.09 0.066±0.001
(7) 213.57±4.09 0.066±0.001

(3) 273.35±1.78 0.071±0.002
(3) 273.35±1.78 0.071±0.002

b)

Rayleigh

c)

NEA6

Figure S9. Joint inversion at NEA6, with a 2.0 km thick sedimentary layer in the initial model (blue in panel c).

9

a)

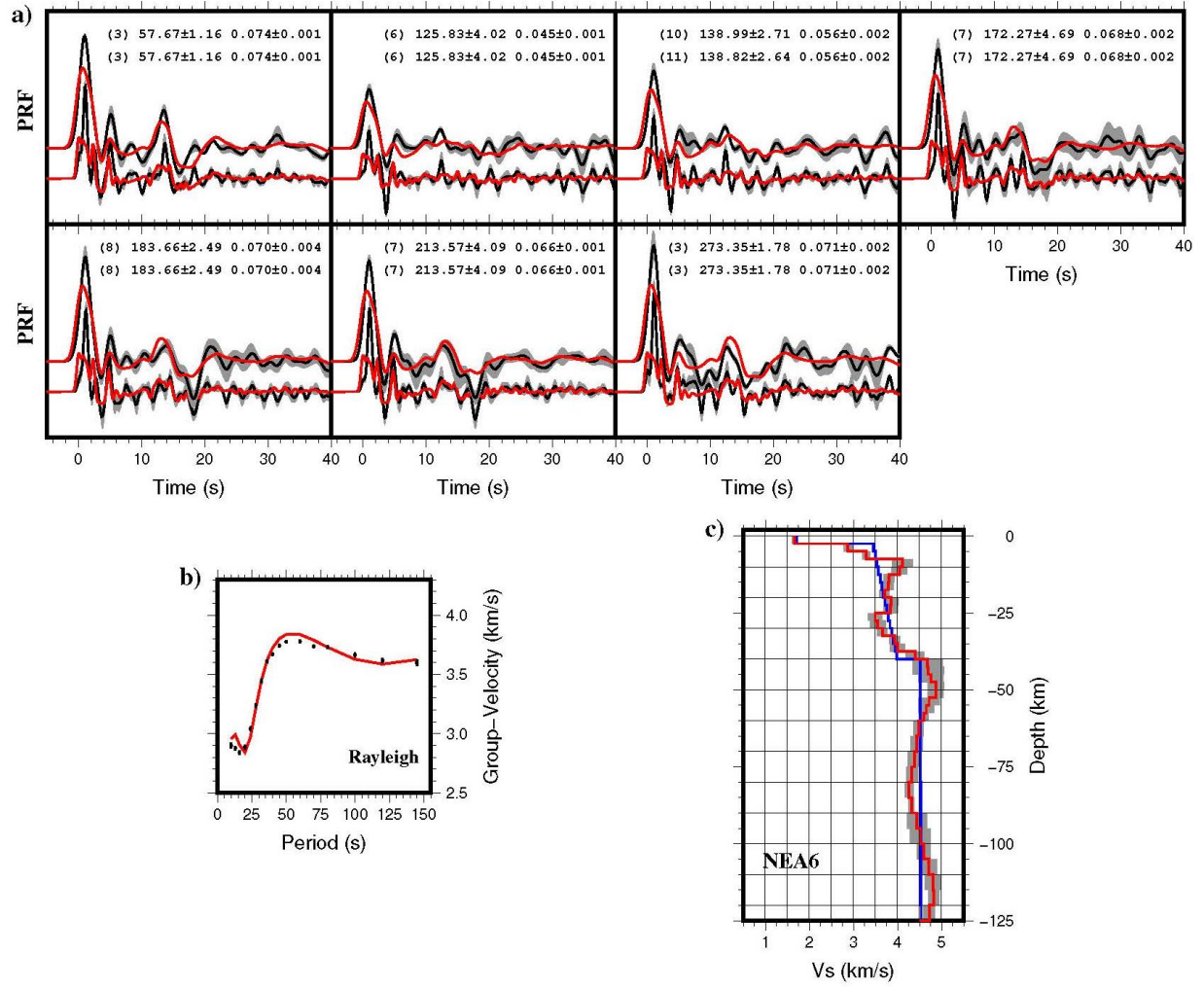(3) 57.67±1.16 0.074±0.001
(3) 57.67±1.16 0.074±0.001

(6) 125.83±4.02 0.045±0.001
(6) 125.83±4.02 0.045±0.001

(10) 138.99±2.71 0.056±0.002
(11) 138.82±2.64 0.056±0.002

(7) 172.27±4.69 0.068±0.002
(7) 172.27±4.69 0.068±0.002

(8) 183.66±2.49 0.070±0.004
(8) 183.66±2.49 0.070±0.004

(7) 213.57±4.09 0.066±0.001
(7) 213.57±4.09 0.066±0.001

(3) 273.35±1.78 0.071±0.002
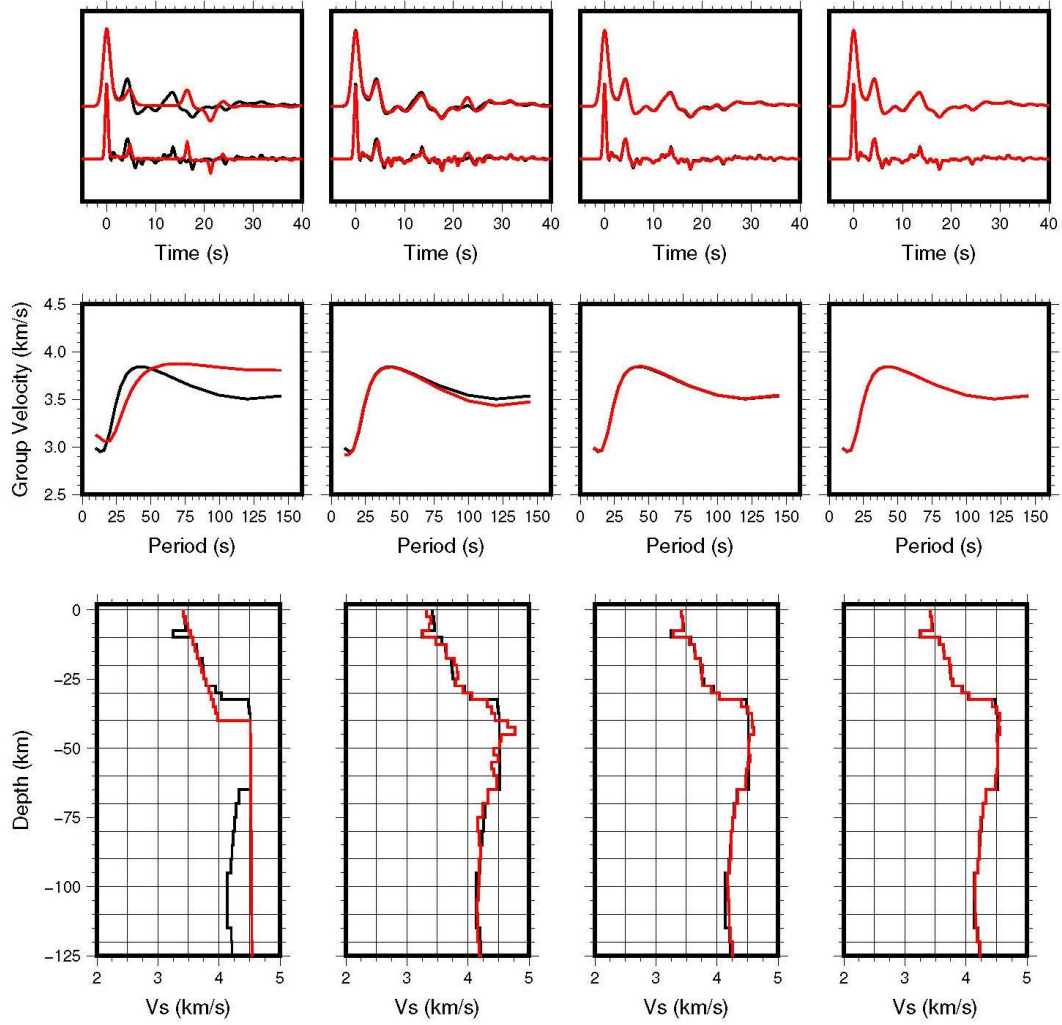(3) 273.35±1.78 0.071±0.002

b)

c)

NEA6

61   Figure S10. Joint inversion at NEA6, with a 2.5 km thick sedimentary layer in the

62   starting model (blue in panel c).

Figure S11. A synthetic joint inversion test. The true model (black) contains a 2.5 km thick low Vs anomaly in the crust and an upper-mantle low shear velocity zone below 65 km depth. The synthetic receiver functions (ray-parameter 0.05 s/km, at Gaussian widths of α = 2.5 and 1.0) and Rayleigh wave group velocity dispersion curve (at periods of 10–145 s) corresponding to the true model are represented by black lines. Evolution of the iterated solutions and the corresponding predicted data are shown by red lines. Note that the resulting model converged to the true solution and the presumed crustal and upper-mantle Vs anomalies are perfectly recovered in three iterations.

72
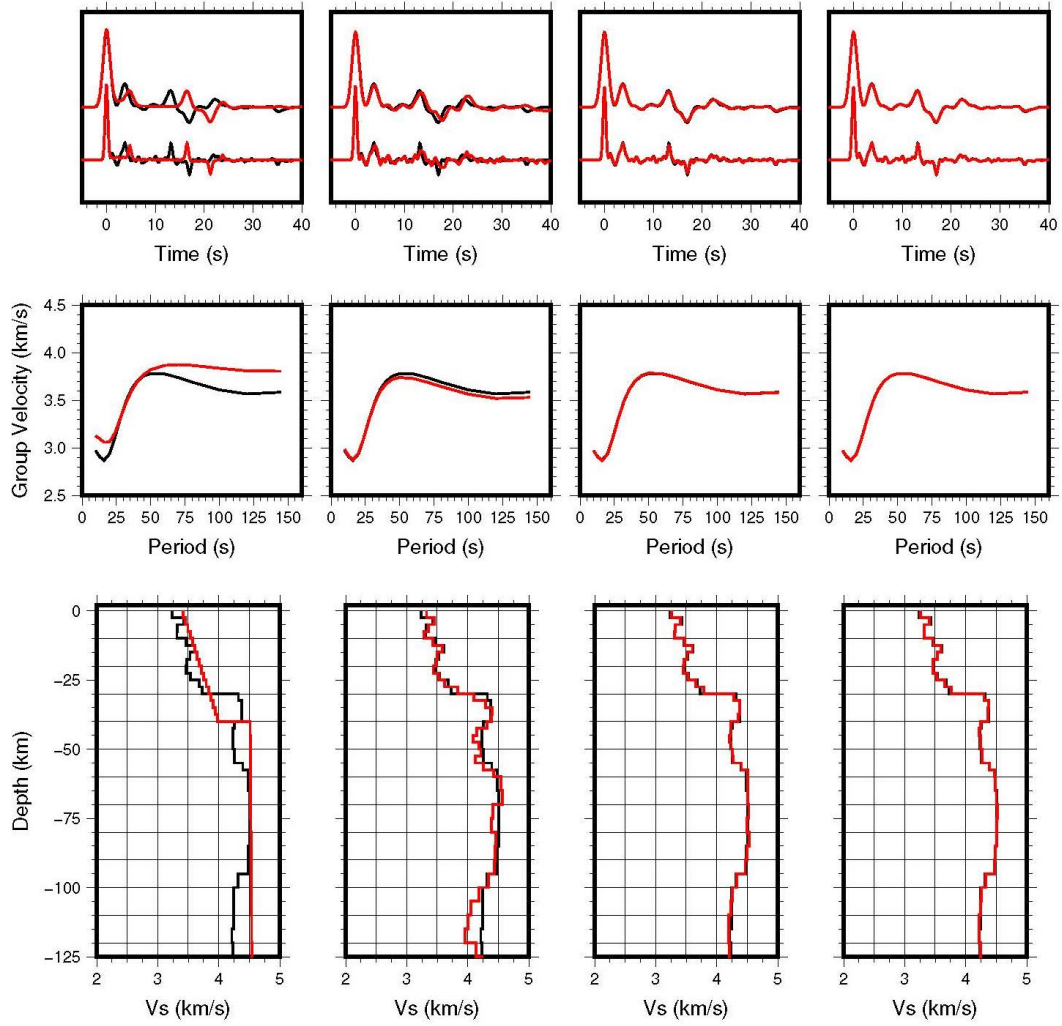
Figure S12. Same as Figure S11, but for a different true model. This true model (black) includes a slow S velocity feature at 40-60 km depths (i.e., uppermost-mantle levels) and an upper-mantle low velocity zone below 95 km. Note that the significant shear velocity anomalies at the crustal and upper-mantle depths are successfully recovered by joint inversion.